Collision expansion for the radiative transport equation: analytical results and numerical simulations

Vadim A. Markel[a,*], Manabu Machida[b] and John C. Schotland[c]

[a]*Department of Radiology, University of Pennsylvania, Philadelphia, Pennsylvania, 19104, USA*
[b]*Department of Informatics, Faculty of Engineering, Kindai University, Higashi-Hiroshima, 739-2116, Japan*
[c]*Department of Mathematics and Department of Physics, Yale University, New Haven, Connecticut, 06520, USA*

ARTICLE INFO

ABSTRACT

We consider the collision expansion of the Green's function of the radiative transport equation (RTE) in an infinite medium. Analytical expressions in terms of quadratures of the most simple form are given for all orders of the expansion. Singularities of the Green's function are considered in detail. While it is well known that the zeroth and first terms in the expansion are singular (and proportional to delta functions), we show that the second order term contains a logarithmic singularity. All higher-order terms are regular. We further establish a relation between the Green's function and the signal measured by a collimated detector. In the presence of singularities, this relation is not always obvious and, at second order, it cannot be stated in a form that is independent of the acceptance angle of the detector. We also consider the density and energy current. Theoretical results are supported by Monte-Carlo simulations.

1. Introduction

The expansion of the Green's function of the radiative transport equation (RTE) in powers of the scattering coefficient (also known as the collision expansion) is a fundamental part of radiative transport theory. It provides an intuitive picture of multiple scattering and leads to useful approximations to the solution of the RTE. The zeroth-order term in the expansion (the ballistic Green's function) describes a ray whose intensity is exponentially attenuated according to the Beer-Lambert law, a result that is widely used in computed X-ray tomography [1, 2]. The first order term describes a broken ray with a scattering vertex. The associated broken-ray transform is utilized in single-scattering tomography [3, 4] and its generalizations [5]. Other applications include remote sensing and recovering the optical parameters of a medium from intensity measurements [6].

The collision expansion is easily derived from the RTE. Nevertheless, its individual terms, in particular, the low-order terms, have a rather complicated mathematical form. An explicit expression for the first-order term was derived by Siewert in 1985 [7] assuming isotropic scattering. In the same work, Siewert pointed out that the first order term is singular. It was widely known that the zeroth-order term is also singular, but the singularity at first order came as a bit of a surprise. In 1998, Bondarenko showed that, in addition to the above singularities, the Green's function of the RTE also contains a logarithmic singularity [8]. It is clear from the results of Ref. [8] that this singularity cannot be attributed to the zeroth and first-order terms, but the second-order term was not derived in [8] explicitly. Expressions for the first-order term were derived in other physical settings

more recently in Refs. [3, 9], and for the vector RTE in Refs. [10, 11].

In spite of all these developments, the theory of the collision expansion is not complete, and there remain important points to be made regarding even the first-order term. In particular, this term contains a delta function, which is defined with respect to a particular axis of symmetry. Indeed, different expressions are obtained in different reference frames. Of course, these expressions predict the same measurable signal. However, the relation between the Green's function and the measurable signal is not obvious. While one might assume naively that the signal measured by a narrowly collimated detector is proportional to the Green's function, this relation cannot hold when the latter is singular. In addition, assuming that the smooth pre-factor in front of the delta function is the measurable signal is, in fact, incorrect. Furthermore, the second-order term has rarely been considered in the literature, and the fact that it contains a logarithmic singularity is not widely known. Even though this singularity is in some sense relatively weak, disregarding it can lead to errors. For example, attempts to compute by numerical integration the contribution of doubly-scattered photons, when the source and detector are collimated in the same plane, yields a manifestly incorrect result.

In this paper, we fill the gaps in the theory mentioned above, derive explicit expressions for all terms in the collision expansion, and reduce these expressions to simple quadratures. In the case of the first-order term, we provide two-different derivations in the reference frames associated with the primary ray and the line of sight. We also establish the relationship between the first-order Green's function and the signal measured by a collimated detector. In addition, we show how these results can be used to compute the density and current of electromagnetic energy. The second-order term can be written in a reference frame-independent

---
*Corresponding author

✉ vmarkel@upenn.edu (V.A. Markel); machida@hiro.kindai.ac.jp (M. Machida); john.schotland@yale.edu (J.C. Schotland)

ORCID(s): 0000-0002-9748-6865 (V.A. Markel); 0000-0002-1830-0760 (M. Machida); 0000-0003-0545-1962 (J.C. Schotland)

form, but still contains a singularity. We show that, near the singularity, the relation between the Green's function and the measurable signal cannot be stated in a general form, but depends in an essential way on the properties of the detector. We also give examples of computing the density and energy current at second order. Higher-order terms can be reduced to relatively simple quadratures. At third and higher orders, these results are of little practical importance due to the computational complexity involved in evaluating the integrals. However, we have applied these results to show that all terms of third order and higher are regular. Therefore, all singularities are contained in the zeroth, first and second order terms.

Throughout the paper, we illustrate our theoretical results with numerical simulations. All examples are obtained for a non-absorbing medium with the Henyey-Greenstein phase function [12]

$$\mathscr{A}(x) = \frac{1}{4\pi} \frac{1 - g^2}{\left(1 - 2gx + g^2\right)^{3/2}} , \qquad (1)$$

where x is the cosine of the scattering angle and g is the scattering asymmetry parameter ($0 \leq g < 1$). We consider two cases: $g = 0.8$, which corresponds to forward-peaked scattering, and $g = 0$, which corresponds to the constant phase function $\mathscr{A}(x) = 1/4\pi$ (isotropic scattering).

Two types of simulations will be presented. In the first type, we have computed the terms in the collision expansion of the Green's function G_n for $n = 1, 2$ by numerical integration. Then we used the numerical values of G_n and the formulas derived below to compute the terms W_n in the expansion of the signal W measured by a narrowly-collimated detector. Note that, at second order, the mathematical relation between W_2 and G_2 cannot be established for some special orientations of the detector. This is due to the logarithmic singularity in G_2. We will also compute the terms in the expansion of the energy density u_n and current $\mathbf{J}_n$, by numerical integration of G_n. The quantities W_n, u_n and $\mathbf{J}_n$ are physically measurable and will be displayed in the figures.

Secondly, to validate the theoretical results of this paper, we have computed the same quantities (W_n, u_n and $\mathbf{J}_n$) by the Monte-Carlo method. We have implemented the standard Monte-Carlo algorithm with an exponential probability density of the step length. The probability density of the new direction upon scattering was determined according to (1). Detection was in a small region δV (location of the detector) characterized by the distance to the primary ray H and projection onto the primary ray L. To accelerate convergence, we have accounted for the cylindrical symmetry of the problem as described in [13]. For the purpose of computing W_n, we counted only the photons arriving in δV with the directional vectors $\hat{\mathbf{s}}$ in the solid angle subtended by the detector. The volumetric detection scheme is algorithmically different from counting the photons that cross the detector surface (which was not introduced explicitly), but the two approaches are approximately equivalent under the conditions reported in the simulations. To compute u_n,

we counted the photons arriving in δV regardless of $\hat{\mathbf{s}}$, and to compute $\mathbf{J}_n$ we counted photons with the weight $\hat{\mathbf{s}}$. To make comparisons with the theory at a given n, we only counted the photons that underwent exactly n scattering events. When our intent was to fully account for multiple scattering, we counted all photons regardless of history, but terminated the trajectories after 10 scattering events. For the chosen geometries, limiting the number of scattering events by 10 was sufficient to obtain convergence.

For simplicity, all formulas below have been obtained for a homogeneous medium. However, the generalization to an inhomogeneous medium is straightforward. The key idea is that formulas containing products of the total attenuation coefficient μ_t and the length of the ray that connects the source and detector, for given positions of the scattering vertices $\mathbf{r}_1, \ldots, \mathbf{r}_n$, must be replaced by integrals of $\mu_t(\mathbf{r})$ along the corresponding trajectory. The factors μ_s^n must be replaced by $\mu_s(\mathbf{r}_1) \cdots \mu_s(\mathbf{r}_n)$. Finally, the phase function can also be made position-dependent without much difficulty. We do not show these results because they require lengthy formulas, whose practical utility beyond first order is unclear.

The paper is organized as follows. In section 2, we introduce the stationary RTE and the collision expansion of its Green's function G. In section 3, we establish the relationship between the Green's function G or the terms in the collision expansion G_n and the signal measured by a collimated detector (W or W_n). Some of the formulas derived in this section are general and some are applicable only if G is a smooth function of the angular variables. In the sections that follow, we utilize the more general expressions in the cases when G is singular. In sections 4 and 5, we consider the first and second orders in the collision expansion, respectively. There we derive and illustrate numerically the terms G_1 and G_2 and the corresponding contributions to the signal measured by a collimated detector, W_1 and W_2. We also compute the density u_n and energy current $\mathbf{J}_n$ ($n = 1, 2$). In section (6), we provide without derivation the expressions for G_n with $n \geq 3$. Finally, section 7 contains a discussion of our results.

2. Collision expansion for the stationary RTE

We consider the stationary RTE

$$\hat{\mathbf{s}} \cdot \nabla I(\mathbf{r}, \hat{\mathbf{s}}) + \mu_t I(\mathbf{r}, \hat{\mathbf{s}}) =$$
$$\mu_s \int \mathscr{A}(\hat{\mathbf{s}} \cdot \hat{\mathbf{s}}') I(\mathbf{r}, \hat{\mathbf{s}}') \, d^2 \hat{s}' + Q(\mathbf{r}, \hat{\mathbf{s}}) , \qquad (2)$$

where $I(\mathbf{r}, \hat{\mathbf{s}})$ is the specific intensity at the point $\mathbf{r}$ in the direction of the unit vector $\hat{\mathbf{s}}$, μ_t is the total attenuation coefficient, μ_s is the scattering coefficient, $\mathscr{A}(x)$ is the scattering phase function, and $Q(\mathbf{r}, \hat{\mathbf{s}})$ is the source. The Green's function $G(\mathbf{r}, \hat{\mathbf{s}}; \mathbf{r}', \hat{\mathbf{s}}')$ gives the specific intensity due to a point-like, ideally collimated source of the form

$$Q(\mathbf{r}, \hat{\mathbf{s}}) = \Delta(\hat{\mathbf{s}}, \hat{\mathbf{s}}') \, \delta(\mathbf{r} - \mathbf{r}') , \qquad (3)$$

where $\Delta(\hat{\mathbf{s}}, \hat{\mathbf{s}}')$ is the angular delta function (defined in Appendix A) and $\delta(\cdot)$ is the usual Dirac delta function. The

collision expansion of the Green's function is of the form

$$G = \sum_{n=0}^{\infty} (G_0 S)^n G_0 = G_0 \sum_{n=0}^{\infty} (SG_0)^n \,, \qquad (4)$$

where S and G_0 are the scattering operator and the zeroth order (ballistic) Green's function [14]. The kernels of these operators are defined as

$$S(\mathbf{r}, \hat{\mathbf{s}}; \mathbf{r}', \hat{\mathbf{s}}') = \mu_s \, \delta(\mathbf{r} - \mathbf{r}') \, \mathscr{A}(\hat{\mathbf{s}} \cdot \hat{\mathbf{s}}') \qquad (5)$$

and

$$G_0(\mathbf{r}, \hat{\mathbf{s}}; \mathbf{r}', \hat{\mathbf{s}}') = \Delta(\hat{\mathbf{s}}, \hat{\mathbf{s}}') \, \Delta(\mathbf{r} - \mathbf{r}', \hat{\mathbf{s}}') \, g(\mathbf{r}, \mathbf{r}') \,, \qquad (6)$$

where

$$g(\mathbf{r}, \mathbf{r}') := \frac{p(\mathbf{r}, \mathbf{r}')}{|\mathbf{r} - \mathbf{r}'|^2} \,, \quad p(\mathbf{r}, \mathbf{r}') := e^{-\mu_t |\mathbf{r} - \mathbf{r}'|} \,. \qquad (7)$$

Note the relation

$$\int G_0(\mathbf{r}, \hat{\mathbf{s}}; \mathbf{r}', \hat{\mathbf{s}}') \, d^2\hat{s} \, d^2\hat{s}' = g(\mathbf{r}, \mathbf{r}') \,. \qquad (8)$$

In what follows, we will compute explicitly (more precisely, reduce to quadratures) all terms in the expansion (4). However, we will pay particular attention to G_1 and G_2, as these terms are amendable to numerical computation, and are singular. To make the resulting expressions more symmetric, we will denote the position and direction of the source by $\mathbf{r}_b$ and $\hat{\mathbf{s}}_b$ and the analogous quantities characterizing the point of observation by $\mathbf{r}_a$ and $\hat{\mathbf{s}}_a$. Thus, we will compute explicitly the functions

$$G_n(\mathbf{r}_a, \hat{\mathbf{s}}_a; \mathbf{r}_b, \hat{\mathbf{s}}_b) = \int G_0(\mathbf{r}_b, \hat{\mathbf{s}}_b; \mathbf{r}_1, \hat{\mathbf{s}}_1) \, S(\mathbf{r}_1, \hat{\mathbf{s}}_1; \mathbf{r}_2, \hat{\mathbf{s}}_2)$$
$$\times \, G_0(\mathbf{r}_2, \hat{\mathbf{s}}_2; \mathbf{r}_3, \hat{\mathbf{s}}_3) \cdots S(\mathbf{r}_{2n-1}, \hat{\mathbf{s}}_{2n-1}; \mathbf{r}_{2n}, \hat{\mathbf{s}}_{2n})$$
$$\times \, G_0(\mathbf{r}_{2n}, \hat{\mathbf{s}}_{2n}; \mathbf{r}_b, \hat{\mathbf{s}}_b) \, d^3 r_1 \cdots d^3 r_{2n} \, d^2\hat{s}_1 \cdots d^2\hat{s}_{2n} \,. \qquad (9)$$

Note that the nth term in (9) contains n copies of the operator S and therefore is proportional to μ_s^n.

3. Measurable signal

We will need to define the relation between the Green's function (or the terms in the collision expansion) and the signal measured by a collimated detector. Assume that the detector is suitably small, located at the point $\mathbf{r}$, with its axis in the direction $\hat{\mathbf{u}}$. Then we can write the power registered by the detector due to a point source with power P_0, located at $\mathbf{r}_b$ and pointing in the direction $\hat{\mathbf{s}}_b$ as

$$P(\mathbf{r}, \hat{\mathbf{u}}) = \eta \, P_0 \, S \int_{\hat{\mathbf{u}} \cdot \hat{\mathbf{s}} > 1 - \beta^2/2} G(\mathbf{r}, \hat{\mathbf{s}}; \mathbf{r}_b, \hat{\mathbf{s}}_b) \, d^2\hat{s} \,, \qquad (10)$$

where S is the detector area, η is its energy conversion efficiency and $\pi \beta^2$ is the solid angle subtended by the detector. Here we view $\mathbf{r}_b$ and $\hat{\mathbf{s}}_b$ as parameters and focus on the

dependence of P on $\mathbf{r}$ and $\hat{\mathbf{u}}$. It is convenient to introduce the dimensionless signal

$$W(\mathbf{r}, \hat{\mathbf{u}}) := \mu_t^{-2} \int_{\hat{\mathbf{u}} \cdot \hat{\mathbf{s}} > 1 - \beta^2/2} G(\mathbf{r}, \hat{\mathbf{s}}; \mathbf{r}_b, \hat{\mathbf{s}}_b) \, d^2\hat{s} \,, \qquad (11)$$

so that

$$P(\mathbf{r}, \hat{\mathbf{u}}) = \eta \, P_0 \, \mu_t^2 \, S \, W(\mathbf{r}, \hat{\mathbf{u}}) \,. \qquad (12)$$

The overall constant $\eta \, P_0 \, \mu_t^2 \, S$ does not depend on $\mathbf{r}$ and $\hat{\mathbf{u}}$ and may not be known in an experiment. We will therefore focus on computing $W(\mathbf{r}, \hat{\mathbf{u}})$. To this end, we will need to evaluate the integral (11) assuming β is small. Consider a reference frame with spherical coordinates r, θ, φ and let the polar and azimuthal angles of $\hat{\mathbf{u}}$ be θ_u and φ_u. Since β is small, the vector $\hat{\mathbf{s}}$ in (11) is close to $\hat{\mathbf{u}}$ and we can write for its angles $\theta = \theta_u + \delta\theta$ and $\varphi = \varphi_u + \delta\varphi$, where $\delta\theta$ and $\delta\varphi$ are small. Then, to lowest nonvanishing order, we have

$$\hat{\mathbf{u}} \cdot \hat{\mathbf{s}} \approx 1 - \frac{1}{2} \left(\delta\theta^2 + \sin^2\theta_u \, \delta\varphi^2 \right) \,. \qquad (13)$$

Using this result, we can rewrite (11) as

$$W(\mathbf{r}, \hat{\mathbf{u}}) \approx \mu_t^{-2} \int_{\theta_u - \beta}^{\theta_u + \beta} \sin\theta \, d\theta \int_{\varphi_u - \alpha(\theta)}^{\varphi_u + \alpha(\theta)} d\varphi \, G(\mathbf{r}, \hat{\mathbf{s}}; \mathbf{r}_b, \hat{\mathbf{s}}_b) \,, \quad (14)$$

where

$$\alpha(\theta) := \frac{\sqrt{\beta^2 - (\theta - \theta_u)^2}}{\sin\theta_u} \,. \qquad (15)$$

If $G(\mathbf{r}, \hat{\mathbf{s}}; \mathbf{r}_b, \hat{\mathbf{s}}_b)$ is a smooth function of $\hat{\mathbf{s}}$, we can replace $\hat{\mathbf{s}}$ by $\hat{\mathbf{u}}$ in the above expressions and write

$$W(\mathbf{r}, \hat{\mathbf{u}}) \approx 2\mu_t^{-2} \, G(\mathbf{r}, \hat{\mathbf{u}}; \mathbf{r}_b, \hat{\mathbf{s}}_b) \int_{\theta_u - \beta}^{\theta_u + \beta} \alpha(\theta) \, \sin\theta \, d\theta \,. \quad (16)$$

Since in the integration domain of (16) $\sin\theta \approx \sin\theta_u$, we can further simplify this expression as

$$W(\mathbf{r}, \hat{\mathbf{u}}) \approx 2\mu_t^{-2} \, G(\mathbf{r}, \hat{\mathbf{u}}; \mathbf{r}_b, \hat{\mathbf{s}}_b) \int_{-\beta}^{\beta} \sqrt{\beta^2 - t^2} \, dt$$
$$= \pi\beta^2 \, \mu_t^{-2} \, G(\mathbf{r}, \hat{\mathbf{u}}; \mathbf{r}_b, \hat{\mathbf{s}}_b) \,. \qquad (17)$$

Thus, the power registered by a collimated detector is proportional to its acceptance solid angle and the specific intensity at the location of the detector and in the direction of axis of collimation $\hat{\mathbf{u}}$. In general, this allows us to view the specific intensity and the corresponding Green's function as measurable quantities under conditions when the approximations adopted above are accurate.

An important point here is that the derivation of equation (17) was based on the assumption that $G(\mathbf{r}, \hat{\mathbf{s}}; \mathbf{r}_b, \hat{\mathbf{s}}_b)$ is a smooth function of $\hat{\mathbf{s}}$. Under this assumption, the result

(17) could be easily anticipated on physical grounds. However, for the first two terms in the collision expansion, the smoothness assumption is not valid. For such functions, the derivation must be carried out more carefully starting from Eq. (14) and, in fact, yields a different result, as will be demonstrated below.

Some types of measurements (e.g., involving wide acceptance angles), as well as physical processes such as fluorescence, are sensitive to the density and current of energy, which are defined as

$$u(\mathbf{r}) = \int G(\mathbf{r}, \hat{\mathbf{s}}; \mathbf{r}_b, \hat{\mathbf{s}}_b) \, d^2\hat{s} \, , \tag{18a}$$

$$\mathbf{J}(\mathbf{r}) = \int G(\mathbf{r}, \hat{\mathbf{s}}; \mathbf{r}_b, \hat{\mathbf{s}}_b) \hat{\mathbf{s}} \, d^2\hat{s} \, . \tag{18b}$$

These quantities are different from $W(\mathbf{r}, \hat{\mathbf{u}})$ and will also be computed below.

4. First-order scattering

The first-order term in the collision expansion is given by (9) with $n = 1$. Using (5), (6), we obtain the following expression:

$$G_1(\mathbf{r}_a, \hat{\mathbf{s}}_a; \mathbf{r}_b, \hat{\mathbf{s}}_b) = \mu_s \mathcal{A}(\hat{\mathbf{s}}_a \cdot \hat{\mathbf{s}}_b) \int g(\mathbf{r}_a, \mathbf{r}) \, g(\mathbf{r}, \mathbf{r}_b)$$
$$\times \Delta(\mathbf{r}_a - \mathbf{r}, \hat{\mathbf{s}}_a) \, \Delta(\mathbf{r} - \mathbf{r}_b, \hat{\mathbf{s}}_b) \, d^3 r \, . \tag{19}$$

We now introduce the change of variables

$$\mathbf{r} = \mathbf{r}_b + \ell \hat{\mathbf{s}} \, , \quad d^3 r = \ell^2 \, d\ell \, d^2\hat{s} \, . \tag{20}$$

Upon integrating over $\hat{\mathbf{s}}$, we are left with the one-dimensional integral

$$G_1(\mathbf{r}_a, \hat{\mathbf{s}}_a; \mathbf{r}_b, \hat{\mathbf{s}}_b) = \mu_s \mathcal{A}(\hat{\mathbf{s}}_a \cdot \hat{\mathbf{s}}_b) \int_0^\infty \frac{d\ell}{w^2(\ell)}$$
$$\times \Delta(\mathbf{w}(\ell), \hat{\mathbf{s}}_a) \exp[-\mu_t(\ell + w(\ell))] \, , \tag{21}$$

where

$$\mathbf{w}(\ell) := \mathbf{r}_{ab} - \ell \hat{\mathbf{s}}_b \, , \quad \mathbf{r}_{ab} := \mathbf{r}_a - \mathbf{r}_b \, , \tag{22}$$

and we have used the definition of the p-function in (7). Even though the integral (21) appears to be simple, it is not easy to compute. As was pointed out by Siewert [7], the result contains a singularity. Below, we will compute G_1 in two different ways.

4.1. Reference frame associated with the primary ray

Consider the rectangular frame shown in Fig. 1. Here the source is located at the origin and the vector $\hat{\mathbf{s}}_b$ is pointing in the positive direction of the Z-axis, so that $\hat{\mathbf{s}}_b = \hat{\mathbf{z}}$. Consequently, the Z-axis coincides with the primary (unscattered) ray. The point of observation $\mathbf{r}_a$ is located at the distance $H > 0$ from the primary ray, and its projection onto the primary ray is L, so that, $\mathbf{r}_{ab} \cdot \hat{\mathbf{s}}_b = L$. Here L can
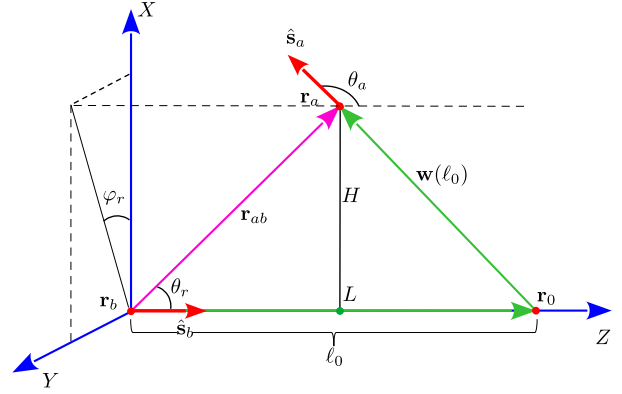

Figure 1: Reference frame associated with the primary beam. The green line is the single-scattered or broken ray with a vertex at $\mathbf{r}_0$.

be positive, negative, or zero. The condition $H > 0$ implies that the point of observation does not lie along the primary ray. We denote by θ_a and φ_a the polar and azimuthal angles of $\hat{\mathbf{s}}_a$ and by θ_r, and φ_r the polar and azimuthal angles of $\mathbf{r}_{ab}$. The angle φ_a is not shown in the drawing. Note that

$$\theta_r = \arctan(H/L) \, . \tag{23}$$

A scattering vertex $\mathbf{r}_0$ exists only if $\theta_a > \theta_r$. Therefore, we immediately see that $G_1(\mathbf{r}_a, \hat{\mathbf{s}}_a; \mathbf{r}_b, \hat{\mathbf{s}}_b) = 0$ if $\theta_a < \theta_r$.

We now use the reference frame-dependent representation of the angular delta function to simplify (21). Let $\theta_w(\ell)$ and $\varphi_w(\ell)$ be the polar and azimuthal angles of the vector $\mathbf{w}(\ell)$ in the reference frame of Fig. 1. Then

$$\Delta\left(\mathbf{w}(\ell), \hat{\mathbf{s}}_a\right) = \delta\left(\varphi_w(\ell) - \varphi_a\right) \delta\left(\cos\theta_w(\ell) - \cos\theta_a\right) \, . \tag{24}$$

It follows from Fig. 1 that

$$\varphi_w(\ell) = \varphi_r \, , \quad \cos\theta_w(\ell) = \frac{L - \ell}{\sqrt{H^2 + (L - \ell)^2}} \, . \tag{25}$$

We can use the above expressions to rewrite (24) as

$$\Delta\left(\mathbf{w}(\ell), \hat{\mathbf{s}}_a\right) = \delta(\varphi_a - \varphi_r) \delta\left(f(\ell)\right) \, , \tag{26}$$

where

$$f(\ell) := \frac{L - \ell}{\sqrt{H^2 + (\ell - L)^2}} - \cos\theta_a \, . \tag{27}$$

If $f(\ell)$ has only simple roots ℓ_k, we have that

$$\delta(f(\ell)) = \sum_k \frac{\delta(\ell - \ell_k)}{|f'(\ell_k)|} \, , \tag{28}$$

where the prime denotes the first derivative. The function $f(\ell)$ defined in (27) has one simple root

$$\ell_0 = L - H \cot\theta_a \tag{29}$$

and no other roots. Using this result, we find that

$$\left| f'(\ell_0) \right| = \frac{\sin^3 \theta_a}{H} \,, \quad w^2(\ell_0) = \frac{H^2}{\sin^2 \theta_a} \,. \tag{30}$$

We thus obtain

$$\Delta\left(\mathbf{w}(\ell), \hat{\mathbf{s}}_a \right) = \frac{H}{\sin^3 \theta_a} \,\delta(\varphi_a - \varphi_r)\,\delta(\ell - \ell_0) \,. \tag{31}$$

Putting everything together, we evaluate the integral in (21) as

$$G_1(\mathbf{r}_a, \hat{\mathbf{s}}_a; \mathbf{r}_b, \hat{\mathbf{s}}_b = \hat{\mathbf{z}}) = \Theta(\theta_a - \theta_r)\,\delta(\varphi_a - \varphi_r)$$
$$\times \frac{\mu_s \,\mathscr{A}(\cos\theta_a)}{H \sin\theta_a}\, \exp\left[-\mu_t \left(L + H\,\frac{1 - \cos\theta_a}{\sin\theta_a} \right) \right] \,. \tag{32}$$

In this expression, $\Theta(x)$ is the step function and the factor $\Theta(\theta_a - \theta_r)$ expresses the condition that the vertex $\mathbf{r}_0$ is on the primary ray; otherwise, the integral in (21) vanishes. Note that the critical angle θ_r is defined to be in the interval $(0, \pi)$, and the branch of the arctangent in (23) must be chosen correspondingly. The argument of the exponent is the optical path along the broken ray $\mathbf{r}_b \to \mathbf{r}_0 \to \mathbf{r}_a$, which is shown in Fig. 1 by the green line segments. We also indicated explicitly that (32) is the restriction for $\hat{\mathbf{s}}_b = \hat{\mathbf{z}}$ of the function $G_1(\mathbf{r}_a, \hat{\mathbf{s}}_a; \mathbf{r}_b, \hat{\mathbf{s}}_b)$. Note that while for every $\hat{\mathbf{s}}_b$, there is a special reference frame in which (32) is correct, this expression cannot be used directly to compute the first-order approximation to the specific intensity for a more general source function. To this end, the expression derived in the next subsection is more convenient.

We see from the above that the first-order Green's function is singular due to the presence of the angular delta function $\delta(\varphi_a - \varphi_r)$. It is important to keep in mind that the angle φ_a is not arbitrary, but is defined as the azimuthal angle of the unit vector $\hat{\mathbf{s}}_a$ in the reference frame of Fig. 1.

4.2. Reference frame associated with the line of sight

Now we repeat the computation of G_1 in the reference frame whose Z-axis coincides with the line of sight, that is, with the ray connecting the source and the point of observation. The relevant geometry is illustrated in Fig. 2. We denote by θ_a, φ_a and θ_b, φ_b the polar and azimuthal angles of the vectors $\hat{\mathbf{s}}_a$ and $\hat{\mathbf{s}}_b$. Note that these are not the same angles as in section 4.1. Also, in contrast to the case where the Z-axis coincides with the primary ray, now both $\hat{\mathbf{s}}_a$ and $\hat{\mathbf{s}}_b$ can vary.

As above, we start from the expression (21) and utilize the coordinate-dependent representation (24) of the angular delta function $\Delta(\mathbf{w}(\ell), \hat{\mathbf{s}}_a)$. In the reference frame of Fig. 2, we have

$$\varphi_w(\ell) = \pi + \varphi_b \,, \tag{33a}$$

$$\cos\theta_w(\ell) = \frac{r_{ab} - \ell \cos\theta_b}{\sqrt{r_{ab}^2 - 2\,\ell\, r_{ab} \cos\theta_b + \ell^2}} \,. \tag{33b}$$
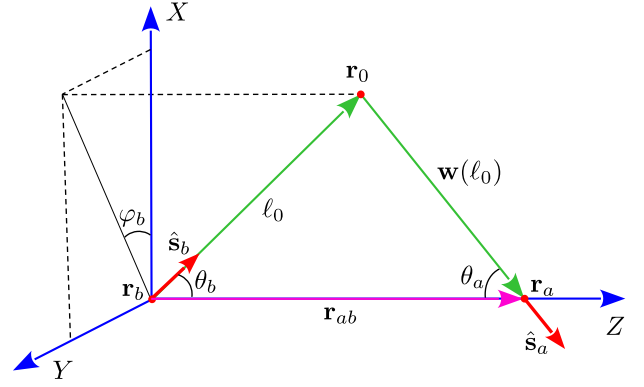

Figure 2: Reference frame associated with the line of sight. The green line is the single-scattered or broken ray with the vertex at $\mathbf{r}_0$.

Therefore, the function $f(\ell)$ in (26) is of the form

$$f(\ell) = \frac{r_{ab} - \ell \cos\theta_b}{\sqrt{r_{ab}^2 - 2\,\ell\, r_{ab} \cos\theta_b + \ell^2}} - \cos\theta_a \,. \tag{34}$$

This function has one simple root

$$\ell_0 = r_{ab}\, \frac{\sin\theta_a}{\sin(\theta_a + \theta_b)} \,. \tag{35}$$

We can verify this result from the triangle $(\mathbf{r}_a, \mathbf{r}_0, \mathbf{r}_b)$ in Fig. 2. We also have

$$\left| f'(\ell_0) \right| = \frac{1}{r_{ab}}\,\frac{\sin\theta_a}{\sin\theta_b}\,\sin^2(\theta_a + \theta_b) \,, \tag{36a}$$

$$w^2(\ell_0) = r_{ab}^2\,\frac{\sin^2\theta_b}{\sin^2(\theta_a + \theta_b)} \,, \tag{36b}$$

$$\hat{\mathbf{s}}_a \cdot \hat{\mathbf{s}}_b = \cos(\theta_a + \theta_b) \,. \tag{36c}$$

Putting everything together, we find

$$G_1(\mathbf{r}_a, \hat{\mathbf{s}}_a; \mathbf{r}_b, \hat{\mathbf{s}}_b) = \Theta(\pi - \theta_a - \theta_b)\,\delta(\pi + \varphi_b - \varphi_a)$$
$$\times \frac{\mu_s \,\mathscr{A}(\cos(\theta_a + \theta_b))}{r_{ab} \sin\theta_a \sin\theta_b}\, \exp\left[-\mu_t\, r_{ab}\,\frac{\sin\theta_a + \sin\theta_b}{\sin(\theta_a + \theta_b)} \right] \,. \tag{37}$$

The step function expresses the condition that ℓ_0 must be positive; otherwise, the integral vanishes. As in section 4.1, the argument of the exponent is the optical path along the broken ray $\mathbf{r}_b \to \mathbf{r}_0 \to \mathbf{r}_a$, although now it is expressed in terms of different geometric quantities. It is easy to see that the optical paths that appear in (32) and (37) are in fact equal. The result (37) was derived in [3] for spatially inhomogeneous media.

4.3. Collimated detector

We now compute the contribution of the first-order term in the collision expansion to the signal. We have from the general relation (14)

$$W_1(\mathbf{r}, \hat{\mathbf{u}}) \approx \mu_t^{-2} \int_{\theta_u - \beta}^{\theta_u + \beta} \sin\theta \, d\theta \int_{\varphi_u - \alpha(\theta)}^{\varphi_u + \alpha(\theta)} d\varphi \, G_1(\mathbf{r}, \hat{\mathbf{s}}; \mathbf{r}_b, \hat{\mathbf{s}}_b) \,. \tag{38}$$

Since $G_1(\mathbf{r}, \hat{\mathbf{s}}; \mathbf{r}_b, \hat{\mathbf{s}}_b)$ is a singular function of $\hat{\mathbf{s}}$, we cannot follow the sequence of approximations that were outlined in section 3, but must evaluate the integral more carefully. To this end, we need a specific expression for $G_1(\mathbf{r}, \hat{\mathbf{s}}; \mathbf{r}_b, \hat{\mathbf{s}}_b)$. Either (32) or (37) can be used and will yield the same result. Without loss of generality, let us start with (32). We immediately notice that $W_1(\mathbf{r}, \hat{\mathbf{u}})$ vanishes unless the collimation axis $\hat{\mathbf{u}}$ lies in the plane of the triangle $(\mathbf{r}_b, \mathbf{r}_0, \mathbf{r}_a)$, within the small solid angle defined by β. We therefore place the detector so that its axis is in the above plane. Then the signal can be parameterized as $W_1(L, H, \theta_u)$, where θ_u is the angle between $\hat{\mathbf{u}}$ and the Z-axis (we have $\cos\theta_u = \hat{\mathbf{z}} \cdot \hat{\mathbf{u}}$). With the above in mind, we substitute the expression (32) into (38) and find that the delta function $\delta(\varphi - \varphi_r)$ can be integrated directly. This is a substantial difference compared with section 3, where the integral over φ was proportional to $2\alpha(\theta)$. Now, due to the presence of the angular delta function in (32), the integral over φ is 1. We then have

$$W_1(L, H, \theta_u) \approx \int_{\theta_u-\beta}^{\theta_u+\beta} \Theta(\theta - \theta_r) \sin\theta \, d\theta$$
$$\times \frac{\mu_s \mathscr{A}(\cos\theta)}{\mu_t^2 H \sin\theta} \exp\left[-\mu_t\left(L + H\frac{1-\cos\theta}{\sin\theta}\right)\right]. \quad (39)$$

It can be seen that the factor of $\sin\theta$ cancels. The remaining function is smooth except at $\theta = \theta_r$. However, this discontinuity can be easily handled. Assuming β is small, we obtain the approximation

$$W_1(L, H, \theta_u) \approx \frac{2\beta \mu_s}{\mu_t^2 H} \Theta(\theta_u - \theta_r) \mathscr{A}(\cos\theta_u)$$
$$\times \exp\left[-\mu_t\left(L + H\frac{1-\cos\theta_u}{\sin\theta_u}\right)\right]. \quad (40)$$

Thus, we see that W_1 is not proportional to the solid angle of acceptance of the detector (rather, the coefficient is 2β), and is not proportional to G_1. In Fig. 3, we provide a numerical verification of this result. Here we plot the function defined in (40) and compare it to Monte-Carlo simulations in which only one scattering event for each photon was taken into account. The correspondence is very good, apart from small statistical fluctuations, which were left intentionally in the data (by keeping the number of photons relatively small) so that the curves could be visually distinguished. We emphasize that inclusion of the factor of $\sin\theta_u$ in the denominator of the formula for W_1, as is suggested by the form of (32) or (37), would not allow us to fit the data.

The quantity shown in Fig. 3 is the first order contribution W_1 to the total signal W. The following question arises: does W_1 approximate W accurately? It so happens that the answer to this question cannot be given in general, but depends on the value of β. For $\beta = 0.02$ and other parameters that were used to generate the data for Fig. 3, the approximation is in fact very good. However, the higher order terms in the expansion of G are smooth functions of $\hat{\mathbf{s}}$ (except for G_2, which must be considered separately). As

was shown in section 3, the contributions of such functions to W scale as $\pi\beta^2$, while the contribution of G_1 scales as 2β. Therefore, for any position of the detector such that there exists a single-scattering vertex, we can choose β to be sufficiently small for W_1 to dominate the total signal W. It follows that, with sufficient collimation, one can always measure W_1. The same is true for the contribution of ballistic (non-scattered) photons as described by W_0. In practice, the possibility of such filtering of scattered light is limited, since the amplitudes of the delta functions in G_0 and G_1 decay exponentially with the source-detector separation. Correspondingly, an exponentially-small collimation angle is required to achieve the effect, which results in an exponentially-weak signal. Here the effects of noise have not been considered.

If measurements of $W_1(L, H, \theta_u)$ are available for several values of L and H, one can determine the optical parameters of the medium including the attenuation coefficient μ_t and the phase function $\mathscr{A}(x)$ by fitting experimental data to the formula (40). It is important to use this expression (without the factor of $\sin\theta_u$ in the denominator) rather than any expression for G_1. Note that the scattering coefficient μ_s cannot be recovered in this manner since it appears in the formula as an overall coefficient. Of course, this approach works only if W_1 is the dominant contribution to W, which can be controlled to some extent by reducing the collimation parameter β. A good indication that W_1 gives the dominant contribution to the measured signal is a sharp transition of the measured power from a finite value to zero at the critical angle θ_r. If there is a discontinuity but the signal past the critical angle is not zero, it can be concluded that multiple scattering is a significant contribution to the signal.

4.4. Density and current

The density and current of energy are defined in (18). The first order contributions to these quantities are defined as

$$u_1(\mathbf{r}) = \int G_1(\mathbf{r}, \hat{\mathbf{s}}; \mathbf{r}_b, \hat{\mathbf{s}}_b) \, d^2\hat{s}, \quad (41a)$$

$$\mathbf{J}_1(\mathbf{r}) = \int G_1(\mathbf{r}, \hat{\mathbf{s}}; \mathbf{r}_b, \hat{\mathbf{s}}_b) \hat{\mathbf{s}} \, d^2\hat{s}. \quad (41b)$$

As in the case of W_1, we can compute the density and current using either (32) or (37) for G_1; it is convenient to start from the former expression. We parameterize u and $\mathbf{J}$ by L and H (see Fig. 1), and substitute (32) into

$$u_1(L, H) = \frac{\mu_s}{H} \int_{\theta_r}^{\pi} \mathscr{A}(\cos\theta) e^{-\mathscr{O}(\theta)} \, d\theta, \quad (42a)$$

$$J_{1z}(L, H) = \frac{\mu_s}{H} \int_{\theta_r}^{\pi} \mathscr{A}(\cos\theta) e^{-\mathscr{O}(\theta)} \cos\theta \, d\theta, \quad (42b)$$

$$J_{1\rho}(L, H) = \frac{\mu_s}{H} \int_{\theta_r}^{\pi} \mathscr{A}(\cos\theta) e^{-\mathscr{O}(\theta)} \sin\theta \, d\theta, \quad (42c)$$

where

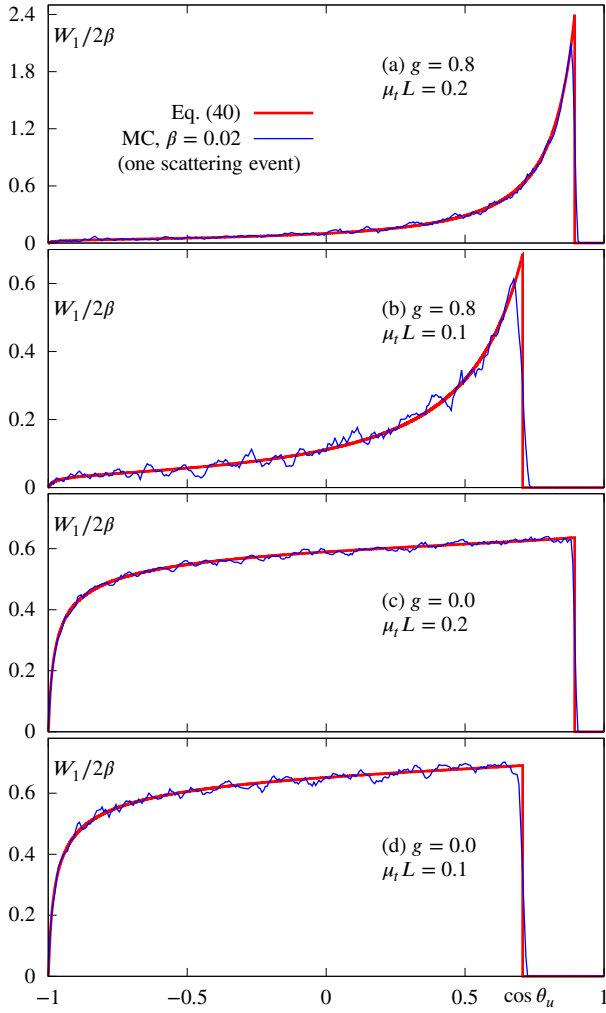$$\mathscr{O}(\theta) = \mu_t\left(L + H\frac{1-\cos\theta}{\sin\theta}\right) \quad (43)$$

Figure 3: First order contribution W_1 to the signal measured by a collimated detector with the axis $\hat{\mathbf{u}}$, normalized to 2β, for an infinite nonabsorbing medium characterized by $\mu_s = \mu_t = \text{const}$ and the Henyey-Greenstein phase function with $g = 0.8$ (a,b) and $g = 0.0$ (c,d). In this figure, W_1 is plotted as a function of $\cos\theta_u$ for $\mu_t H = 0.1$ (in all cases) and $\mu_t L = 0.2$ (a,c) and $\mu_t L = 0.1$ (b,d). Here θ_u is the angle between the axis of the detector and the Z-axis. See Fig. 2 for an illustration of the applicable geometry. Thick red lines represent the analytical result (40) and thin blue lines represent Monte-Carlo simulations accounting for exactly one scattering event. For the MC simulations, the detector acceptance parameter was set to $\beta = 0.02$.

is the optical path along the broken ray with the exit direction θ in a homogeneous medium with the attenuation coefficient μ_t. We denote by J_{1z} the Cartesian component of $\mathbf{J}_1$ along the Z-axis and by $J_{1\rho}$ the radial component (in the direction perpendicular to the Z axis).

The expressions (42) are too complicated to evaluate analytically. However, the integrals can be easily computed numerically. Several examples of computations of u_1 and $\mathbf{J}_1$ are shown in Figs. 4,5 and 6 for the same media as in Fig. 3. However, for u and $\mathbf{J}$, there is no angular dependence

to display. Instead, we plot the quantities of interest as functions of L for two different fixed values of H. For comparison, we also plot in these figures the total density and current u and $\mathbf{J}$ computed by Monte-Carlo simulations accounting for up to 10 scattering events, which is enough for convergence for all parameters considered. It can be seen that, at $\mu_t H = 0.1$, the first-order approximation is only moderately accurate. However, Cartesian components of the current are approximated better than the density. This is in agreement with the observation made above, namely, that, with sufficient collimation, one can measure directly W_1 even under the conditions when multiple scattering is not negligible. Indeed, computation of the current can be regarded as weak collimation. At $\mu_t H = 0.01$, the accuracy of the first-order approximation is quite good for all three quantities that are displayed in Figs. 4-6. Note that here we consider much larger values of L than in Fig. 3. In general, one can expect the quality of approximation to decrease as we move further away from the source.

We conclude this section with the following observation. The radial component of the current $J_{1\rho}$ is nonnegative. However, J_{1z} changes sign and has a negative minimum. In a homogeneous nonamplifying medium, this property of $\mathbf{J}$ is generally true and not specific to the first-order approximation. However, the minimum can be shallow and difficult to see, as is the case in Panel (c) of Fig. 5.

5. Second-order scattering

The second-order term in the collision expansion is defined by (9) with $n = 2$. Upon integration, we obtain the expression

$$G_2(\mathbf{r}_a, \hat{\mathbf{s}}_a; \mathbf{r}_b, \hat{\mathbf{s}}_b) = \mu_s^2 \int g(\mathbf{r}_a, \mathbf{r}_1)\, g(\mathbf{r}_1, \mathbf{r}_2)\, g(\mathbf{r}_2, \mathbf{r}_b)$$
$$\times \Delta(\mathbf{r}_a - \mathbf{r}_1, \hat{\mathbf{s}}_a)\, \mathscr{A}(\hat{\mathbf{s}}_a \cdot \hat{\mathbf{s}})\, \Delta(\hat{\mathbf{s}}, \mathbf{r}_1 - \mathbf{r}_2)$$
$$\times \mathscr{A}(\hat{\mathbf{s}} \cdot \hat{\mathbf{s}}_b)\, \Delta(\hat{\mathbf{s}}_b, \mathbf{r}_2 - \mathbf{r}_b)\, d^3r_1\, d^3r_2\, d^2\hat{s}\,. \quad (44)$$

We now make the change of variables

$$\mathbf{r}_1 = \mathbf{r}_a + \ell_1 \hat{\mathbf{s}}_1\,, \quad d^3r_1 = \ell_1^2\, d\ell_1\, d^2\hat{s}_1\,,$$
$$\mathbf{r}_2 = \mathbf{r}_b + \ell_2 \hat{\mathbf{s}}_2\,, \quad d^3r_2 = \ell_2^2\, d\ell_2\, d^2\hat{s}_2\,.$$

Integrating out the remaining delta functions, we obtain

$$G_2(\mathbf{r}_a, \hat{\mathbf{s}}_a; \mathbf{r}_b, \hat{\mathbf{s}}_b) = \mu_s^2 \int_0^\infty \int_0^\infty \frac{d\ell_1 d\ell_2}{w^2(\ell_1, \ell_2)} e^{-\mu_t[\ell_1 + \ell_2 + w(\ell_1, \ell_2)]}$$
$$\times \mathscr{A}\left(\hat{\mathbf{s}}_a \cdot \hat{\mathbf{w}}(\ell_1, \ell_2)\right) \mathscr{A}\left(\hat{\mathbf{w}}(\ell_1, \ell_2) \cdot \hat{\mathbf{s}}_b\right)\,. \quad (45)$$

In this expression,

$$\mathbf{w}(\ell_1, \ell_2) := \mathbf{r}_{ab} - (\ell_1 \hat{\mathbf{s}}_a + \ell_2 \hat{\mathbf{s}}_b)\,, \quad (46)$$

and $\hat{\mathbf{w}} = \mathbf{w}/w$ is the unit vector in the direction of $\mathbf{w}$. The relevant geometrical objects are illustrated in Fig. 7. Note that the three vectors $\mathbf{r}_{ab}$, $\hat{\mathbf{s}}_a$ and $\hat{\mathbf{s}}_b$ are not necessarily restricted to a plane.
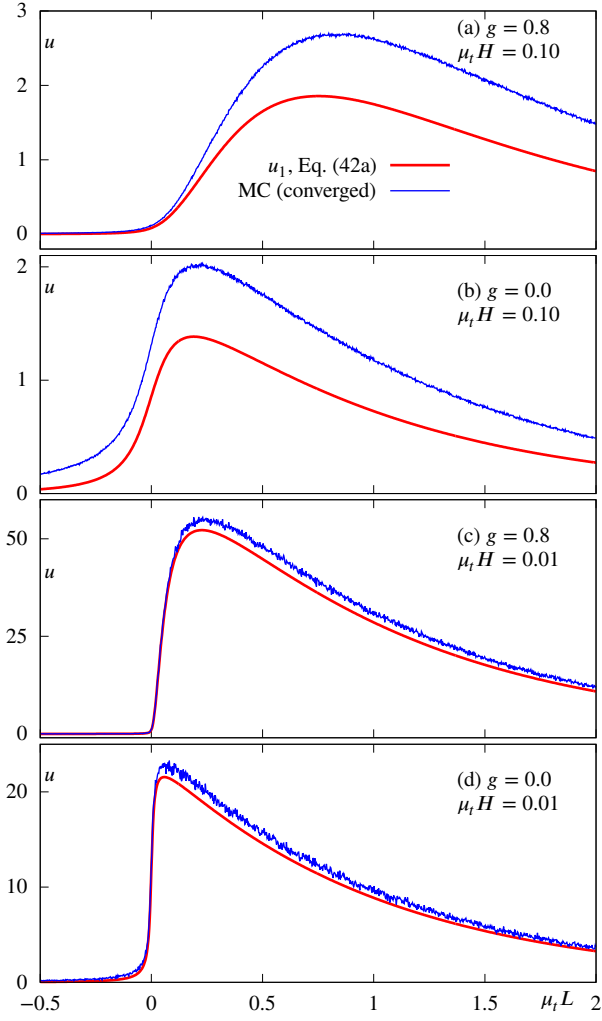
Figure 4: The first-order term u_1 in the collision expansion of the energy density as a function of L for $\mu_t H = 0.1$ (a,b) and $\mu_t H = 0.01$ (c,d) in the same media as in Fig. 3 with the scattering asymmetry parameter $g = 0.8$ (a,c) and $g = 0$ (b,d). Thick red lines show the results of numerical integration according to (42a). Thin blue lines show for comparison the total energy density u computed by Monte-Carlo simulations with up to 10 scattering events, which is enough for convergence in all cases.

5.1. Logarithmic singularity

For some values of the parameters $(\mathbf{r}_a, \hat{\mathbf{s}}_a; \mathbf{r}_b, \hat{\mathbf{s}}_b)$, the function $w^2(\ell_1, \ell_2)$ can vanish in the domain of integration in (45). In this case, the integral diverges, and $G_2(\mathbf{r}_a, \hat{\mathbf{s}}_a; \mathbf{r}_b, \hat{\mathbf{s}}_b)$ is not defined. To analyze the resulting singularity, it is convenient to express the vector $\mathbf{r}_{ab}$ in the following form:

$$\mathbf{r}_{ab} = \bar{\ell}_1 \hat{\mathbf{s}}_a + \bar{\ell}_2 \hat{\mathbf{s}}_b + \mathbf{h}, \quad \text{where } \mathbf{h} \cdot \hat{\mathbf{s}}_a = \mathbf{h} \cdot \hat{\mathbf{s}}_b = 0 . \quad (47)$$

Assuming $\sin \theta_{ab} \neq 0$ (otherwise, the two lines $(\mathbf{r}_a, \mathbf{r}_1)$ and $(\mathbf{r}_b, \mathbf{r}_2)$ in Fig. 7 are parallel and $w^2(\ell_1, \ell_2)$ never vanishes), the parameters $\bar{\ell}_1$ and $\bar{\ell}_2$ are defined uniquely as

$$\bar{\ell}_1 = r_{ab} \frac{\cos \theta_a - \cos \theta_b \cos \theta_{ab}}{\sin^2 \theta_{ab}} , \quad (48a)$$
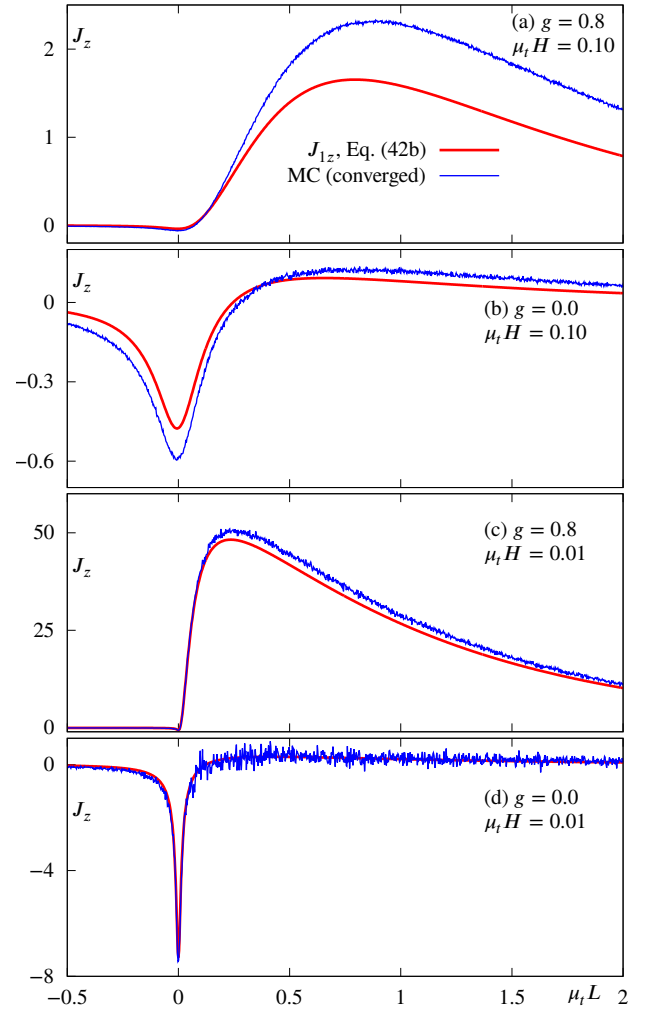
Figure 5: Same as in Fig. 4 but for the z-component of the current of energy, J_z. Thick red lines have been computed by numerical integration according to (42b).

$$\bar{\ell}_2 = r_{ab} \frac{\cos \theta_b - \cos \theta_a \cos \theta_{ab}}{\sin^2 \theta_{ab}} , \quad (48b)$$

where $\cos \theta_a = \hat{\mathbf{s}}_a \cdot \hat{\mathbf{r}}_{ab}$, $\cos \theta_b = \hat{\mathbf{s}}_b \cdot \hat{\mathbf{r}}_{ab}$, $\cos \theta_{ab} = \hat{\mathbf{s}}_a \cdot \hat{\mathbf{s}}_b$ (see Fig. 7). Note that $\bar{\ell}_1$ and $\bar{\ell}_2$ can be positive or negative. Substituting (47) into (46), we find that

$$\mathbf{w}(\ell_1, \ell_2) = (\bar{\ell}_1 - \ell_1) \hat{\mathbf{s}}_a + (\bar{\ell}_2 - \ell_2) \hat{\mathbf{s}}_b + \mathbf{h} . \quad (49)$$

We can further use (48) to compute the length of $\mathbf{h}$. A straightforward calculation yields

$$h^2 = \frac{r_{ab}^2}{\sin^2 \theta_{ab}} \left(\sin^2 \theta_{ab} + 2 \cos \theta_{ab} \cos \theta_a \cos \theta_b - \cos^2 \theta_a - \cos^2 \theta_b \right) . \quad (50)$$

Geometrically, h is the distance between the two lines that cross the points $\mathbf{r}_a$ and $\mathbf{r}_b$ and are collinear with the directional vectors $\hat{\mathbf{s}}_a$ and $\hat{\mathbf{s}}_b$, respectively. This distance is shown in Fig. 7 by a blue line segment. If the three vectors $\hat{\mathbf{s}}_a$, $\hat{\mathbf{s}}_b$ and
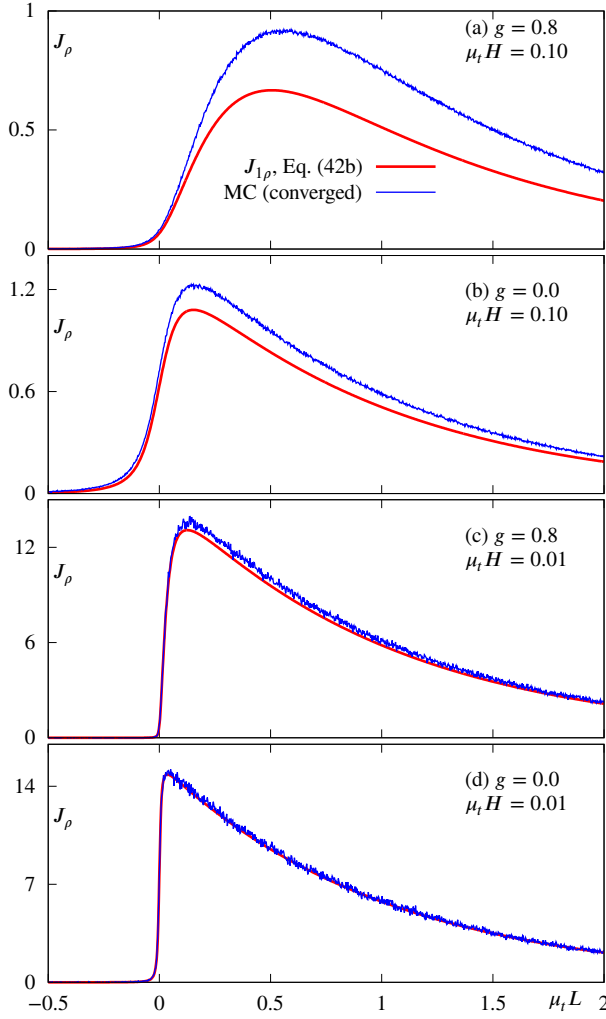
Figure 6: Same as in Fig. 4 but for the radial component of the current of energy, J_ρ. Thick red lines have been computed by numerical integration according to (42c).

$\mathbf{r}_{ab}$ are in the same plane (equivalently, if $\theta_a + \theta_b + \theta_{ab} = \pi$), the two lines intersect and, correspondingly, $\mathbf{h} = 0$. If, in addition, $\bar{\ell}_1, \bar{\ell}_2 > 0$, we have

$$\mathbf{r}_1(\bar{\ell}_1) = \mathbf{r}_2(\bar{\ell}_2) = \mathbf{r}_0 ,\qquad (51)$$

where $\mathbf{r}_0$ is the single-scattering vertex. Existence of the single scattering vertex is the sufficient and necessary condition under which the integral (45) diverges and $G_2(\mathbf{r}_a, \hat{\mathbf{s}}_a; \mathbf{r}_b, \hat{\mathbf{s}}_b)$ is not defined. We can also make the following equivalent statement. The function $G_2(\mathbf{r}_a, \hat{\mathbf{s}}_a; \mathbf{r}_b, \hat{\mathbf{s}}_b)$ is defined if and only if its arguments are such that $G_1(\mathbf{r}_a, \hat{\mathbf{s}}_a; \mathbf{r}_b, \hat{\mathbf{s}}_b) = 0$.

We can prove the above statement and at the same time gain additional insight into the nature of the singularity as follows. Assume that $\bar{\ell}_1, \bar{\ell}_2 > 0$. If at least one of these parameters is negative, the function $w^2(\ell_1, \ell_2)$ does not vanish in the domain of integration in (45). We then introduce the new integration variables $\eta_1 = \ell_1 - \bar{\ell}_1$, $\eta_2 = \ell_2 - \bar{\ell}_2$ and a small region σ in the (η_1, η_2) plane centered at
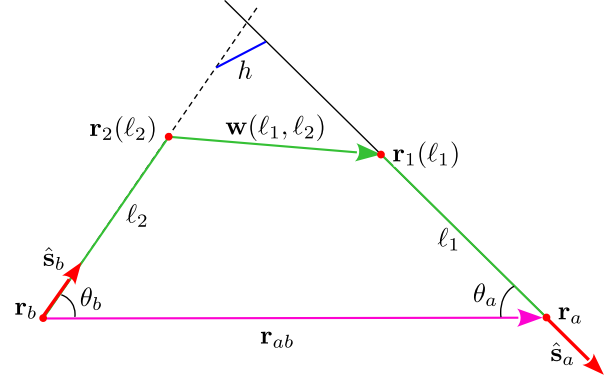

Figure 7: Illustrating the geometry of second-order scattering.

the origin,

$$\sigma := \{\eta_1, \eta_2 \ : \ (\eta_1\hat{\mathbf{s}}_a + \eta_2\hat{\mathbf{s}}_b)^2 \le R^2\} ,\qquad (52)$$

where R is a constant. We can always choose R to be sufficiently small so that σ is entirely contained in the integration domain. The contribution of the integration region σ to G_2 can be written as

$$G_2^{(\sigma)}(\mathbf{r}_a, \hat{\mathbf{s}}_a; \mathbf{r}_b, \hat{\mathbf{s}}_b) = \mu_s^2\, C\, e^{-\mu_t(\bar{\ell}_1 + \bar{\ell}_2)}$$
$$\times \int_\sigma \frac{d\eta_1\, d\eta_2}{(\eta_1\hat{\mathbf{s}}_a + \eta_2\hat{\mathbf{s}}_b)^2 + h^2} ,\qquad (53)$$

where C is a positive constant bounded from below and above by the minimum and maximum over σ of the function

$$F(\eta_1, \eta_2) := \mathscr{A}\left(\hat{\mathbf{s}}_a \cdot \hat{\mathbf{w}}(\bar{\ell}_1 + \eta_1, \bar{\ell}_2 + \eta_2)\right)$$
$$\times \mathscr{A}\left(\hat{\mathbf{w}}(\bar{\ell}_1 + \eta_1, \bar{\ell}_2 + \eta_2) \cdot \hat{\mathbf{s}}_b\right)$$
$$\times \exp\left\{-\mu_t\left[\eta_1 + \eta_2 + w(\bar{\ell}_1 + \eta_1, \bar{\ell}_2 + \eta_2)\right]\right\} .\qquad (54)$$

Note that, in the case $h = 0$, the function $F(\eta_1, \eta_2)$ does not have a limit when $\eta_1, \eta_2 \to 0$. This is because the unit vector $\hat{\mathbf{w}}(\bar{\ell}_1, \bar{\ell}_2) = \mathbf{h}/h$ is not defined for $\mathbf{h} = 0$. We can also say that, when the two scattering vertices $\mathbf{r}_1$ and $\mathbf{r}_2$ coalesce into the single vertex $\mathbf{r}_0$, the scattering angles and the phase functions that depend on these angles become undefined (except for the constant phase function). However, the function $F(\eta_1, \eta_2)$ is positive and bounded from above and below, and therefore has a positive minimum and a positive maximum in the compact set σ. This shows that the constant C that appears in (53) is well defined.

We can now compute the integral (53) analytically, This yields

$$G_2^{(\sigma)}(\mathbf{r}_a, \hat{\mathbf{s}}_a; \mathbf{r}_b, \hat{\mathbf{s}}_b) = \frac{\pi \mu_s^2\, C}{\sin\theta_{ab}}\, e^{-\mu_t(\bar{\ell}_1 + \bar{\ell}_2)}$$
$$\times \ln\left[1 + (R/h)^2\right] .\qquad (55)$$

We thus see that $G_2(\mathbf{r}_a, \hat{\mathbf{s}}_a; \mathbf{r}_b, \hat{\mathbf{s}}_b)$ diverges as $-\ln h$ when $h \to 0$. This singularity is integrable. Indeed, we have

$$\int_0^R \ln\left[1 + (R/h)^2\right] dh = R\left(\pi/2 + \ln 2\right) .\qquad (56)$$
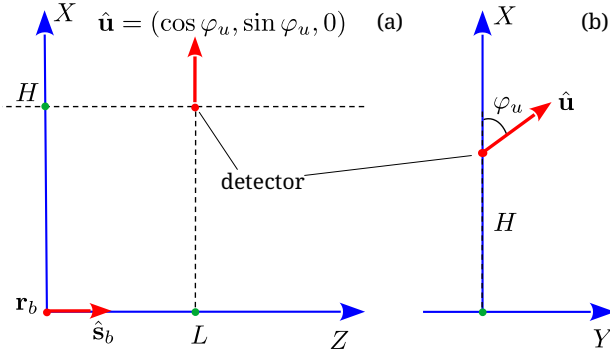
Figure 8: Illustrating the geometry used in Figs. 9, 10 and 11. Panel (a) shows the XZ plane looking into the negative Y-direction and Panel (b) shows the XY plane looking into the positive Z-direction.

Figure 9: Second-order contribution to the signal, W_2, normalized to the acceptance solid angle $\pi\beta^2$ in the same medium as in Fig. 3, as a function of L for $\mu_t H = 0.1$ and several fixed values of φ_u as labeled. Thick red lines have been computed according to (57) and then using numerical integration to evaluate G_2 according to (45). Thin blue lines have been obtained by Monte-Carlo simulations in which only double-scattered photons were counted and the detector acceptance parameter was set to $\beta = 0.02$.

5.2. Collimated detector

It follows from the results of section 3 that, sufficiently far from the singularity, the second-order contribution to the signal is given by

$$W_2(\mathbf{r}, \hat{\mathbf{u}}) = \pi\beta^2 \, \mu_t^{-2} \, G_2(\mathbf{r}, \hat{\mathbf{u}}; \mathbf{r}_b, \hat{\mathbf{s}}_b) \,. \qquad (57)$$

Thus, W_2 is proportional to the acceptance solid angle of the detector $\pi\beta^2$. Near the singularity, the dependence on β may be different, but is not expected to be as slowly varying as 2β, which is characteristic of W_1. To illustrate these statements, we have computed G_2 by numerical integration and compared the results predicted by the formula (57) to Monte-Carlo simulations in which only double-scattered photons were counted. The measurement geometry is illustrated in Fig. 8. We assume that the primary ray coincides with the Z-axis of a rectangular frame, the source is at the origin, and the distance H from the primary ray to the point of observation is fixed. The directional vector $\hat{\mathbf{u}}$ has zero projection onto Z, but can rotate in the XY plane making the angle φ_u with the X-axis.

In Fig. 9, we plot W_2 as a function of L for several fixed nonzero azimuthal angles φ_u. The curves shown in this figure describe a detector with a fixed direction of collimation, which is scanned along the horizontal dotted line in Fig. 8(a). The thick red curves were obtained by numerical integration according to (57) and (45), and the thin blue curves by Monte-Carlo simulations in which only double-scattered photons were counted. The agreement is excellent (small fluctuations were left in the Monte-Carlo data intentionally), even for $\varphi_u = 0.05\pi$, which is close to the singularity. The theoretical curves are smooth with a maximum located somewhere between $\mu_t L = 0$ and $\mu_t L = 1$, depending on φ_u. For larger values of φ_u, the values of W_2 are smaller, and the maximum is less pronounced. At negative values of L (behind the source), the values of W_2 are relatively small since the corresponding second-order trajectories entail significant exponential decay. The
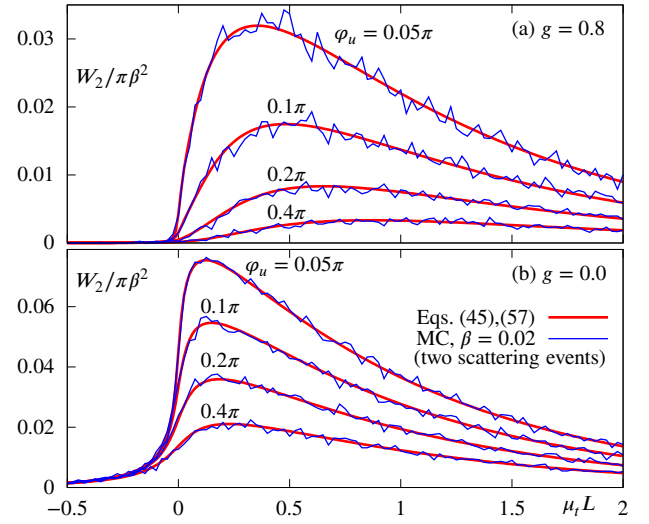
transition at $L = 0$ is more pronounced when $g = 0.8$, since the phase function in this case is forward-peaked.

Fig. 9 does not address the case when the detector axis intersects the primary ray exactly when the function $G_2(\mathbf{r}, \hat{\mathbf{u}}; \mathbf{r}_b, \hat{\mathbf{s}}_b)$ is not defined and (57) is not applicable. For this orientation of the detector, it is difficult to express W_2 in terms of G_2. In particular, the dependence of W_2 on β is more complicated than just a multiplicative factor. In Fig. 10, we show the results of Monte-Carlo simulations of W_2 for $\varphi_u = 0$ and different values of β. It is obvious that W_2 is not proportional to $\pi\beta^2$. Normalizing instead to 2β would yield curves that are even further apart. Moreover, the curves in Fig. 10 do not differ by a multiplicative factor, although this relation holds approximately in a limited range of L. It can also be seen that the numerical values of W_2 in Fig. 10 are substantially larger than those in Fig. 9 (by about a factor of 6). This is due to the contribution of the singularity. Still, for the values of β considered, we have $W_2(\mathbf{r}, \hat{\mathbf{u}}) \ll W_1(\mathbf{r}, \hat{\mathbf{u}})$, assuming that $\hat{\mathbf{u}}$ intersects the primary ray (compare Fig. 10 to Fig. 3 and note the different normalization factors).

Another way to illustrate the logarithmic singularity is to consider the angular dependence of W_2. In Fig. 11, we plot W_2 as a function of φ_u in a small interval of angles, which includes the singularity at $\varphi_u = 0$. Outside of this interval, the function is relatively small and varies slowly. Thick red lines show computations according to (57) where $G_2(\mathbf{r}, \hat{\mathbf{u}}; \mathbf{r}_b, \hat{\mathbf{s}}_b)$ was computed by numerical integration according to (45). As can be seen, this function diverges at $\varphi_u = 0$. Thin blue curves were obtained by Monte-Carlo simulations in which
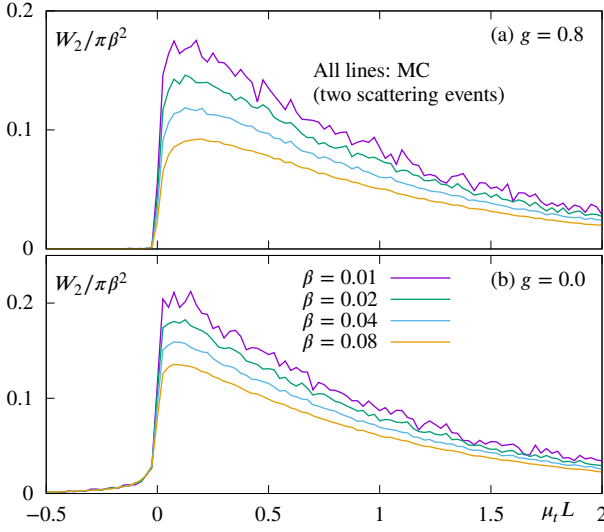
Figure 10: Second-order contribution to the signal, W_2, normalized to the acceptance solid angle $\pi\beta^2$ as a function of L computed at $\varphi_u = 0$, so that the axis of the detector intersects the primary beam. As $G_2(\mathbf{r}, \hat{\mathbf{u}}; \mathbf{r}_b, \hat{\mathbf{s}}_b)$ is in this case not defined, we show the results of Monte-Carlo simulations in which only double-scattered photons were counted by detectors with different values of β. The lines for $\beta = 0.01$ are noisy due to insufficient statistical averaging. $\mu_t H = 0.1$.

Figure 11: Second-order contribution to the signal, W_2, normalized to the acceptance solid angle $\pi\beta^2$ as a function of φ_u (in a small interval centered at $\varphi_u = 0$) for $\mu_t H = 0.1$ and several fixed values of $\mu_t L$ as labeled. Thick red lines have been computed according to (57) and then using numerical integration to evaluate G_2 according to (45). Thin blue lines have been obtained by Monte-Carlo simulations in which only double-scattered photons were counted and the detector acceptance parameter was set to $\beta = 0.02$.

only doubly-scattered photons were counted. The agreement between the two methods is excellent except close to the singularity. Even though (57) is inapplicable for $L > 0$ and $\varphi_u = 0$, W_2 is still a finite and continuous function. However, the value of $W_2(\varphi_u = 0)$ depends on the detector parameter β. In particular, the data of Fig. 11 were computed using $\beta = 0.02$. For $L < 0$, the single-scattering vertex does not exist, and the theoretical curves are continuous at $\varphi_u = 0$. We have illustrated this fact for $\mu_t L = -0.01$, which is quite close to zero, but sufficient to demonstrate the point. For negative values of $\mu_t L$ that are further away from zero, G_2 is still continuous but too small to be displayed in the same plots.

5.3. Density and current

The first order contributions to the density and energy current were considered in section 4.4 above. We now turn to the second-order contributions, which are defined as the angular integrals

$$u_2(\mathbf{r}) := \int G_2(\mathbf{r}, \hat{\mathbf{s}}; \mathbf{r}_b, \hat{\mathbf{s}}_b) \, d^2\hat{s} , \qquad (58a)$$

$$\mathbf{J}_2(\mathbf{r}) := \int G_2(\mathbf{r}, \hat{\mathbf{s}}; \mathbf{r}_b, \hat{\mathbf{s}}_b) \hat{\mathbf{s}} \, d^2\hat{s} . \qquad (58b)$$

Note that $u_2(\mathbf{r})$ and $\mathbf{J}_2(\mathbf{r})$ are continuous and have no singularities. However, numerical computation of these functions is much harder than at first order. Indeed, (58) involves a four-fold integration, which must be carried out for every value of $\mathbf{r}$. This task is possible, but should be approached with care. It is convenient to work in the geometry of Fig. 8,
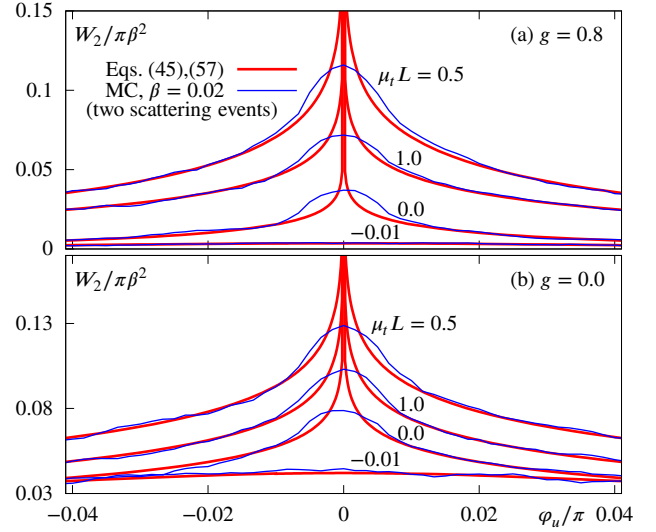
where the source is placed at the origin and illuminates the positive direction of the Z-axis, so that $\mathbf{r}_b = 0$ and $\hat{\mathbf{s}}_b = \hat{\mathbf{z}}$, while the point of observation is $\mathbf{r} = (L, 0, H)$. Some technical details of numerical integration applicable to this geometry are described in Appendix B.

We show examples of the functions $u_2(\mathbf{r})$, $\mathbf{J}_2(\mathbf{r})$ computed by numerical integration in Fig. 12. Here the setup is similar to that used in section 4.4 and Figs. 4-6, except that now we consider only the case $\mu_t H = 0.1$ since, at $\mu_t H = 0.01$, the terms $u_1(\mathbf{r})$ and $\mathbf{J}_1(\mathbf{r})$ already provide an accurate approximation to the total energy density and current and the second order terms are relatively negligible. In Figs. 13, 14 and 15, we plot the sums $u_1 + u_2$ and $\mathbf{J}_1 + \mathbf{J}_2$ for $\mu_t H = 0.1$ and compare the results to those obtained by Monte-Carlo simulation accounting for up to 10 scattering events, which is sufficient for convergence (the same thin blue curves as in Fig. 4, Panels (a) and (b)). It can be seen that the sum of the first two terms in the collision expansion provides a much better approximation than just the first term. In the case $g = 0.8$, the first two terms provide an accurate approximation to all displayed quantities for $\mu_t L < 0.5$ and to J_ρ in the whole range of L considered. In the case $g = 0$, J_z is accurately captured in the whole range of L, but J_ρ and u are not. The remaining discrepancies are explained by the contribution of higher-order terms in the collision expansion. In the geometry considered, these contributions are relatively small but not negligible. Of course, if we move the detector further away from the the source, the
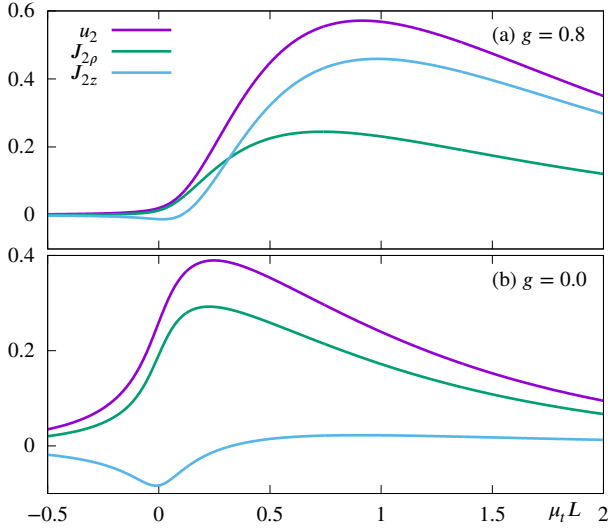
Figure 12: Second-order contributions to the density and energy current u_2 and $\mathbf{J}_2$ computed by numerical integration according to (58) and (45). Here the density u_2 and the components of the current $J_{2\rho}$ (radial) and J_{2z} (along Z) are shown as functions of L for $\mu_t H = 0.1$ and for the same values of the scattering asymmetry parameter g that were considered previously.

higher-order terms will become dominant, and the low-order approximations to $\mathbf{u}(\mathbf{r})$ and $\mathbf{J}(\mathbf{r})$ will lose validity.

6. Third- and higher-order terms

The third-order term in the expansion of the Green's function can be expressed in terms of quadratures by integrating out all the angular delta functions. Here we omit the intermediate steps and show the final result, which is of the form

$$G_3(\mathbf{r}_a, \hat{\mathbf{s}}_a; \mathbf{r}_b, \hat{\mathbf{s}}_b) = \mu_s^3 \int_0^\infty \int_0^\infty \int_0^\infty d\ell_1\, d\ell_2\, d\ell_3 \int_{4\pi} d^2\hat{u}$$
$$\times \frac{e^{-\mu_t(\ell_1+\ell_2+\ell_3+w)}}{w^2}\, \mathscr{A}(\hat{\mathbf{s}}_a \cdot \hat{\mathbf{w}})\, \mathscr{A}(\hat{\mathbf{w}} \cdot \hat{\mathbf{u}})\, \mathscr{A}(\hat{\mathbf{u}} \cdot \hat{\mathbf{s}}_b)\,, \quad (59)$$

where

$$\mathbf{w} := \mathbf{r}_{ab} - (\ell_1 \hat{\mathbf{s}}_a + \ell_2 \hat{\mathbf{s}}_b + \ell_3 \hat{\mathbf{u}})\,. \quad (60)$$

Various quantities appearing in (59) are illustrated geometrically in Fig. 16.

Although (59) is not complicated, it contains a 5-fold integration and cannot be further simplified analytically. For this reason, the expression is unlikely to be of practical utility. However, we can show that $G_3(\mathbf{r}_a, \hat{\mathbf{s}}_a; \mathbf{r}_b, \hat{\mathbf{s}}_b)$ contains no singularities. Indeed, fix $\hat{\mathbf{u}}$ and consider integration over three-dimensional space of vectors $\boldsymbol{\rho} = (\ell_1, \ell_2, \ell_3)$. Assume that $\mathbf{w}(\boldsymbol{\rho}_0) = 0$. Since $\mathbf{w}$ is linear in $\boldsymbol{\rho}$, the factor $1/w^2$ diverges near $\boldsymbol{\rho}_0$ not stronger than $|\boldsymbol{\rho} - \boldsymbol{\rho}_0|^{-2}$. Other factors in the integrand are bounded. It is therefore easy to see that
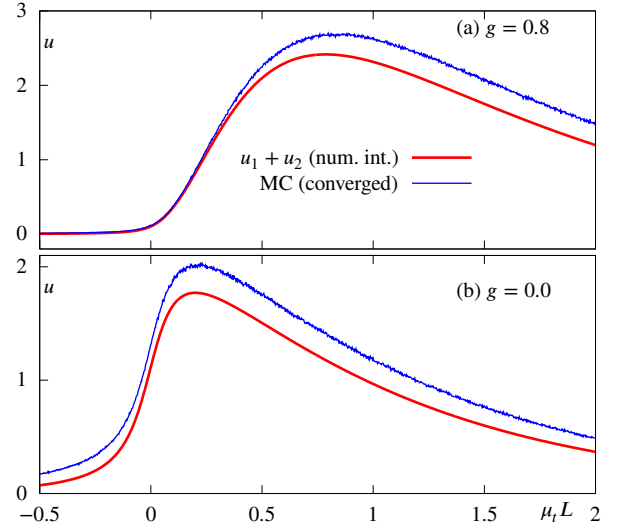

Figure 13: Thick red lines show the sums of the first and second order terms in the collision expansion of the density of energy, $u_1 + u_2$, computed by numerical integration for $\mu_t H = 0.1$. Thin blue lines are the same as in Fig. 4(a,b) and show the results of Monte Carlo simulations for the total density u accounting for up to 10 scattering events, which is sufficient for convergence. The curves with $\mu_t H = 0.01$ (shown in Panels (c) and (d) in Fig. 4) are not included in this figure since, in this case, $u_1 + u_2$ and u are very close and cannot be visually distinguished.
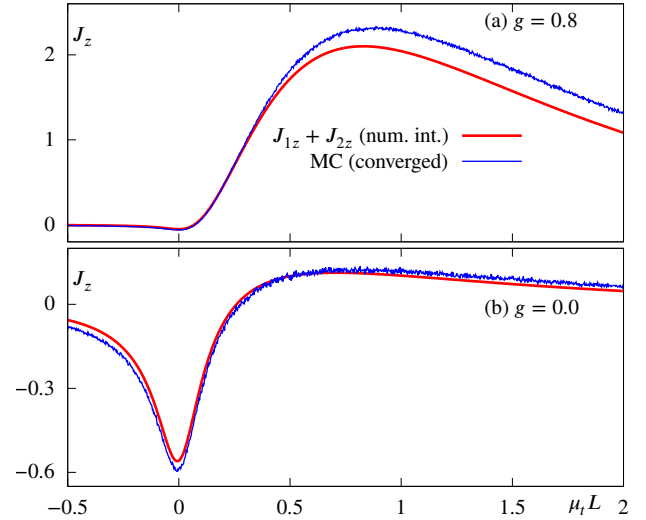

Figure 14: Same as in Fig. 13 but for the Z-component of the current of energy, J_z.

the integral

$$\int_\sigma \frac{d^3\rho}{|\boldsymbol{\rho} - \boldsymbol{\rho}_0|^2} \quad (61)$$

converges. Here σ is a small region containing $\boldsymbol{\rho}_0$. Consequently, $G_3(\mathbf{r}_a, \hat{\mathbf{s}}_a; \mathbf{r}_b, \hat{\mathbf{s}}_b)$ is well defined and finite for all values of its arguments.
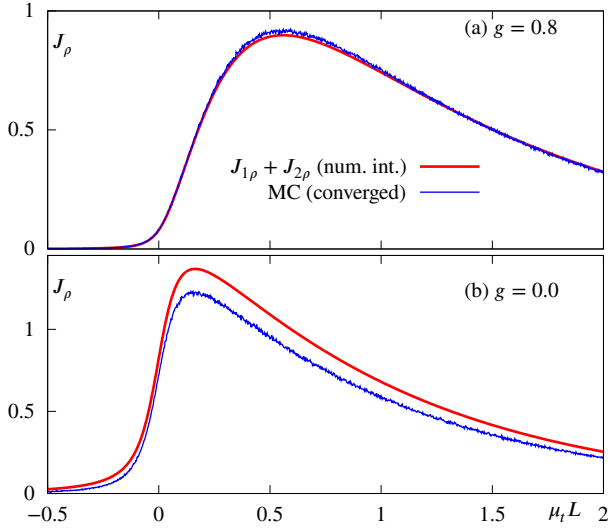
Figure 15: Same as in Fig. 13 but for the radial component of the current of energy, J_ρ.
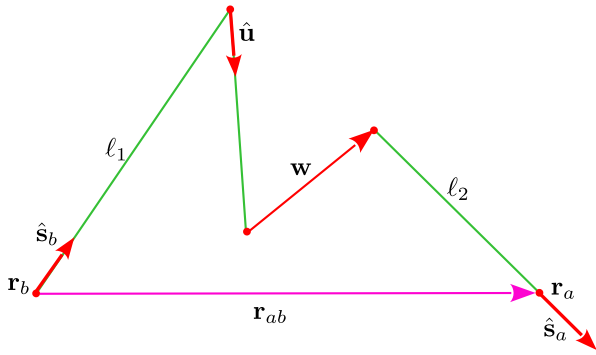

Figure 16: . Illustrating the geometry of third-order scattering. Note that the various points and line segments appearing in the drawing are not necessarily in the same plane.

We can find the expression for G_n of arbitrary order n by adding more line segments to Fig. 16 and including the corresponding terms to (59). In this manner, we obtain for $n > 3$:

$$G_n(\mathbf{r}_a, \hat{\mathbf{s}}_a; \mathbf{r}_b, \hat{\mathbf{s}}_b) = \mu_s^n \int d\ell_1 \, ... \, d\ell_n \, d^2\hat{u}_1 \, ... \, d^2\hat{u}_{n-2}$$

$$\times \frac{1}{w^2} e^{-\mu_t(\ell_1 + ... + \ell_n + w)}$$

$$\times \mathscr{A}(\hat{\mathbf{s}}_a \cdot \hat{\mathbf{w}}) \, \mathscr{A}(\hat{\mathbf{w}} \cdot \hat{\mathbf{u}}_1) \, \mathscr{A}(\hat{\mathbf{u}}_1 \cdot \hat{\mathbf{u}}_2) \, ... \, \mathscr{A}(\hat{\mathbf{u}}_{n-2} \cdot \hat{\mathbf{s}}_b) \, , \quad (62)$$

where

$$\mathbf{w} := \mathbf{r}_{ab} - \left(\ell_1 \hat{\mathbf{s}}_a + \ell_2 \hat{\mathbf{s}}_b + \ell_3 \hat{\mathbf{u}}_1 + \, ... \, + \ell_{n-2} \hat{\mathbf{u}}_{n-2} \right) \, . \quad (63)$$

By the same arguments as above, we can see that G_n is not singular. Of course, evaluating (62) by a numerical quadrature is impractical; one should instead use stochastic methods such as Monte-Carlo integration.

7. Discussion

The mathematical difficulties encountered in calculating the terms in the collision expansion for the RTE are related to the presence of singularities. At first order, the singularity in G_1 has the form of a delta function, whose argument depends on a choice of reference frame. Therefore, in order to derive a formula for G_1, one must specify the reference frame. There are two logical choices: a frame associated with the primary ray and a frame associated with the line of sight. The formulas for G_1 in these two frames are different. However, both predict the same measurable signal W_1 for a collimated detector. To see that this is indeed the case, one must establish the relation between G_1 and W_1 that is valid when G_1 is singular. The presence of the delta function means that W_1 is defined as a convolution of G_1 with a mollifier. Assuming the detector is cylindrically symmetric and accepts incoming rays in a small solid angle with the axis of symmetry $\hat{\mathbf{u}}$, it is possible to compute W_1 analytically. While the expression for W_1 itself is independent of the reference frame, to derive it, we must start in one of the frames mentioned above and compute the convolution by integrating over the solid angle. If one intends to use measurements of W_1 to recover the optical parameters of the medium, it is important to use the correct analytical expression for the quantity W_1.

At second order, the singularity is logarithmic. Although it is in some sense weak, it is also more difficult to handle mathematically. In particular, when the axis of the detector $\hat{\mathbf{u}}$ is close to the direction at which G_1 is singular, it is not possible to state a general relation between W_2 and G_2. Rather, W_2 also depends on the acceptance angle of the detector in a complicated manner.

All higher-order terms G_n with $n \geq 3$ are regular. As a result, the relation between W_n and G_n can be reduced to simple proportionality, with $W_n = \pi\beta^2 \mu_t^{-1} G_n$. For large source-detector separations, when the low-order terms G_0, G_1 and G_2 yield a negligible contribution to the total Green's function G, there exists an approximate relation $W = \pi\beta^2 \mu_t^{-1} G$. One can conclude that, under these conditions, the Green's function (or, more broadly, the specific intensity) is measurable. However, close to the source where the singularities are non-negligible, G is not directly measurable.

Research data for this article

Simulated data that were used in the figures above as well as scripts that can be used to generate all figures from the data (except for the figures containing geometrical sketches) are available in the dataset CollExp (Mendeley Data, V1, doi:10.17632/9c9b8sdrrs.1).

References

[1] F. Natterer, The Mathematics of Computerized Tomography, Wiley, 1986.
[2] T. M. Buzug, Computed Tomography, Springer, 2011, pp. 311–342.
[3] L. Florescu, J. C. Schotland, V. A. Markel, Single-scattering optical tomography, Phys. Rev. E 79 (2009) 036607.

[4] L. Florescu, J. C. Schotland, V. A. Markel, Single-scattering optical tomography: Simultaneous reconstruction of scattering and absorption, Phys. Rev. E 81 (2010) 016602.

[5] F. Zhao, J. C. Schotland, V. A. Markel, Inversion of the star transform, Inverse Problems 30 (2014) 105001.

[6] N. J. McCormick, Methods for solving inverse problems for radiation transport – an update, Transp. Th. Stat. Phys. 15 (1986) 759–772.

[7] C. E. Siewert, On the singular components of the solution to the searchlight problem in raiative transfer, J. Quant. Spectrosc. Radiat. Transfer 33 (1985) 551–554.

[8] A. N. Bondarenko, The structure of the fundamental solution of the time-independent transport equation, J. Math. Anal. Appl. 221 (1998) 430–451.

[9] M. A. Ramirez-Cabrera, C. A. Arancibia-Bulnes, P. J. Valades-Pelayo, The first-order scattering approximation: A closed-form extension to Beer's law, accurate for weakly scattering media, J. Quant. Spectrosc. Radiat. Transfer 262 (2021) 107412.

[10] P. Hank, A. Liemert, A. Kienle, Analytical solution of the vector radiative transfer equation for single scattered radiance, J. Opt. Soc. Am. A 39 (2022) 2045–2053.

[11] P. Hank, A. Liemert, A. Kienle, Analytical solution of the vector radiative transfer equation for the double scattered radiance of semi-infinite media containing polydisperse particle distributions, J. Quant. Spectrosc. Radiat. Transfer 304 (2023) 108605.

[12] L. G. Henyey, J. L. Greenstein, Diffuse radiation in the galaxy, Astrophys. J. 93 (1941) 70–83.

[13] L. Wang, S. L. Jacques, L. Zheng, MCML – Monte Carlo modeling of light transport in multi-layered tissues, Comp. Meth. Prog. Biomed. 47 (1995) 131–146.

[14] R. Carminati, J. C. Schotland, Principles of Scattering and Transport of Light, Cambridge Univ. Press, 2021.

A. Angular delta function

In the literature on radiative transport theory, it is common to denote the angular delta function of two vectors $\mathbf{u}$ and $\mathbf{v}$ as $\delta(\hat{\mathbf{u}} - \hat{\mathbf{v}})$, where $\hat{\mathbf{u}} = \mathbf{u}/u$, $\hat{\mathbf{v}} = \mathbf{v}/v$, and $u = |\mathbf{u}|$, $v = |\mathbf{v}|$. Although, in most cases, this notation can be used without incurring an error, the minus sign in the argument should not be interpreted literally as an algebraic operation. This precaution is important when $\mathbf{u}$ or $\mathbf{v}$ are expressed in terms of other variables. In such cases, the minus sign in $\delta(\hat{\mathbf{u}} - \hat{\mathbf{v}})$ should be treated as a symbol separating two mathematically-independent arguments. We account for this observation explicitly by introducing the notation $\Delta(\mathbf{u}, \mathbf{v})$. Here $\mathbf{u}$ and $\mathbf{v}$ are not restricted to being unit vectors. However, since $\Delta(\mathbf{u}, \mathbf{v}) = \Delta(\hat{\mathbf{u}}, \hat{\mathbf{v}})$, we often use the latter form (sometimes, the arguments of an angular delta function are unit vectors by definition). In the paper, we denote the usual Dirac delta function by $\delta(\cdot)$ and its dimension is implied from the dimension of its argument. For example, $\delta(\mathbf{r})$ is a three-dimensional delta function and $\delta(x)$ a one-dimensional delta function. However, the angular delta function is denoted by $\Delta(\cdot, \cdot)$, and its arguments are always a pair of three-dimensional vectors. Below, we provide a more detailed definition.

Consider the three-dimensional delta function $\delta(\cdot)$. Here the argument in the parenthesis can be any expression that evaluates to a three-dimensional vector. For example, $\delta(\mathbf{u} - \mathbf{v})$ is a function of the shift $\mathbf{u} - \mathbf{v}$. If $\mathbf{v} = \mathbf{u} - \mathbf{w}$, then $\delta(\mathbf{u} - \mathbf{v}) = \delta(\mathbf{w})$. In other words, algebraic operations inside the argument of this delta function are allowed. In a

rectangular reference frame XYZ, we can also write

$$\delta(\mathbf{u} - \mathbf{v}) = \delta(u_x - v_x)\,\delta(u_y - v_y)\,\delta(u_z - v_z)\,, \qquad (64)$$

and the above property is retained. However, it is lost if spherical coordinates are used. Indeed, let (u, θ_u, φ_u) be the length and the polar and azimuthal angles of $\mathbf{u}$, and similarly for $\mathbf{v}$. We have

$$\delta(\mathbf{u} - \mathbf{v}) = \frac{\delta(u - v)}{u^2} \sum_{n=-\infty}^{\infty} \delta(\varphi_u - \varphi_v + 2\pi n)$$
$$\times\ \delta(\cos\theta_u - \cos\theta_v)\,. \qquad (65)$$

Note that summation over n is necessary if φ_u or φ_v can take values outside of the interval $[0, 2\pi]$. It can be seen that the function depends on $\cos\theta_u - \cos\theta_v$ rather than on $\theta_u - \theta_v$.

Now, the second and third functions in (65) can be combined in a single notation:

$$\Delta(\mathbf{u}, \mathbf{v}) := \sum_{n=-\infty}^{\infty} \delta(\varphi_u - \varphi_v + 2\pi n)\,\delta(\cos\theta_u - \cos\theta_v)\,.$$
$$(66)$$

Since $\Delta(\mathbf{u}, \mathbf{v})$ depends on the directions of $\mathbf{u}$ and $\mathbf{v}$ but not on their magnitudes, we have

$$\Delta(\mathbf{u}, \mathbf{v}) = \Delta(\hat{\mathbf{u}}, \mathbf{v}) = \Delta(\mathbf{u}, \hat{\mathbf{v}}) = \Delta(\hat{\mathbf{u}}, \hat{\mathbf{v}})\,. \qquad (67)$$

An important point is that the notation $\Delta(\hat{\mathbf{u}}, \hat{\mathbf{v}})$ can be used independently of reference frame; it is not specific to spherical coordinates. In other words, (66) provides a particular expression for $\Delta(\hat{\mathbf{u}}, \hat{\mathbf{v}})$ in spherical coordinates, but there exist other equivalent expressions. In fact, the angular delta function is completely defined by the following reference frame-independent relations:

$$\Delta(\mathbf{u}, \mathbf{v}) = \Delta(\mathbf{v}, \mathbf{u})\,, \qquad (68a)$$

$$\int \Delta(\mathbf{u}, \mathbf{v})\,\mathrm{d}^2\hat{v} = \int \Delta(\mathbf{u}, \mathbf{v})\,\mathrm{d}^2\hat{u} = 1\,, \qquad (68b)$$

$$\int f(\mathbf{v})\,\Delta(\mathbf{u}, \mathbf{v})\,\mathrm{d}^2\hat{v} = f(v\,\hat{\mathbf{u}})\,. \qquad (68c)$$

Here $\mathrm{d}^2\hat{v}$ is an element of solid angle and $\mathrm{d}^3 v$ is an element of volume. The following relation follows from (68)

$$\int f(\mathbf{v})\,\Delta(\mathbf{u}, \mathbf{v})\,\mathrm{d}^3 v = \int_0^\infty f(v\,\hat{\mathbf{u}})\,v^2\,\mathrm{d}v\,. \qquad (69)$$

We finally note that for the angular delta functions there is no analog of the identity $\delta(\beta x) = |\beta|^{-1}\delta(x)$.

B. Quasi-uniform sampling of the unit sphere for numerical computation of u_2 and $\mathbf{J}_2$.

Assume that a procedure for computing $G_2(\mathbf{r}, \hat{\mathbf{s}}; \mathbf{r}_b, \hat{\mathbf{s}}_b)$ is available. The feasibility of this computation was demonstrated in section 5.2 above. In order to evaluate (58) numerically, we must sample $\hat{\mathbf{s}}$ on the unit sphere as uniformly as possible, and with sufficient density to capture the angular

dependence of G_2. Yet it is important not to use any discrete values of $\hat{s}$ for which G_2 is not defined. One algorithm to achieve such sampling is described below.

Let the polar and azimuthal angles of $\hat{s}$ in the reference frame of Fig. 8 be θ and φ. First, we sample the variable $c = \cos\theta$ in the interval $[-1, 1]$. The samples are $c_n = -1 + \alpha n$, $n = 0, 1, ..., N$, where $\alpha = 2/N$ and N is a sufficiently large even integer (the last condition is important). Then, at each value of n, we sample the angle φ in the interval $[0, 2\pi]$ as follows:

$$\varphi_{nm} = \beta_n (m - 1/2), \quad m = 1, 2, \ldots, M_n, \qquad (70a)$$

where

$$M_n = \begin{cases} 2n + 1, & m \leq N/2 \\ 2(N - n) + 1, & m > N/2 \end{cases}, \qquad (70b)$$

$$\beta_n = 2\pi / M_n. \qquad (70c)$$

Note that $M_0 = M_N = 1$, so that there is only one sample at the North and South poles of the unit sphere. The number of samples on the equator is $N + 1$. Generally, the number of samples on each discrete line of latitude is proportional to its length, so that the sampling is quasi-uniform. Also, the samples φ_{nm} defined by (70a) are all nonzero and therefore we have avoided computing G_2 in the directions of $\hat{s}$ for which it is not defined. To evaluate the integrals in (58), we compute the integrands at the discrete values $\hat{s}_{nm}$, multiply the results by the weights $w_n \alpha \beta_n$ (where $w_0 = w_N = 1/2$ and $w_n = 1$ for all other n) and sum the numbers thus obtained over all n and m. The following identity,

$$\sum_{n=0}^{N} \sum_{m=1}^{M_n} w_n \alpha \beta_n = 4\pi, \qquad (71)$$

confirms that we have described a correct quadrature. Note that the density of sampling of the unit sphere is controlled by the single parameter N.